The effect of source/drain extension asymmetry on the leakage current of ohmicly-contacted carbon nanotube FETs

Khairul Alam and Roger Lake
LAboratory for Terascale and Terahertz Electronics
Department of Electrical Engineering
University of California, Riverside, CA 92521-0204

ABSTRACT

Geometry dependency of the leakage current is investigated by modeling the effects of source/drain extension asymmetry on the leakage current of a 20 nm wrap-around gated ohmicly contacted carbon nanotube field effect transistor (CNTFET). Interband tunneling plays an important role to control the leakage current in CNTFETs. Asymmetric gate structure with gate close to the source blocks much of interband tunneling. The interband component of the leakage current as a percentage of the OFF current reduces from 98.8% to 0.16%, the ON/OFF current ratio increases from 1.4×10^4 to 1.9×10^6, the gate capacitance increases from 0.2 aF to 0.41 aF, and the cut-off frequency decreases from 25 THz to 15 THz with symmetric to asymmetric gate structure.

Keywords: carbon nanotube (CNT), leakage current, asymmetric gate structure, source/drain extension, coulomb blockade

1 INTRODUCTION

Since its discovery in 1991 by the Japanese electron microscopist Sumio Iijima, carbon nanotube (CNT) has been the promising candidate for future nanoelectronics. CNT is essentially one monolayer thick graphene sheet rolled-up into a cylinder. Electron confinement in the radial and circumferential directions makes CNT a one dimensional (1D) nanowire. Better performance of CNT based devices over the conventional MOSFETs has been projected at the scaling limit [1]. CNTFETs with ohmic palladium contact to intrinsic p-type channel have been demonstrated [2–5]. Studies on doping to CNT using potassium [6], modification of metal-CNT work function using chemical means [7, 8], ambipolar conduction in CNT [9–12], and geometry dependent performance [13, 14] of CNTFETs have been investigated.

Also there has been progress in self-assembled functionalized CNTFETs using biological molecule such as DNA. Because of its low inherent conductance in biological environment, DNA properties need to be modified by metallization to facilitate electron transport. Metallization of DNA with gold, silver, copper, palladium, and platinum has been demonstrated [15]. Keren *et. al* have fabricated CNTFETs by self-assembled DNA-templated gold wires and have measured their electrical characteristics [16].

CNTFETs show different scaling behavior than conventional MOSFETs [12, 17, 18], and the OFF current increases exponentially with the drain voltage. This leakage current results from both the interband and intraband tunnelings. The sources of leakage are strongly geometry dependent. Although a self-aligned process has been demonstrated [5], we have found this to *not* be the optimal geometry for minimizing leakage. In this work, we investigate the geometry dependence of the leakage current by modeling the effect of source/drain extension asymmetry on the leakage current of CNTFETs with 20 nm wrap-around gates. The key idea is to produce different electric field in the source and drain contacts so that unwanted tunneling (interband tunneling) can be suppressed to reduce the OFF current. Similar studies have been done both theoretically [19] and experimentally [20], but their theoretical model uses a semiclassical approach under WKB approximation. Our simulation model solves the full-band quantum transport equations self-consistently with Poisson equation.

2 SIMULATION MODEL

Our simulation model is based on a self-consistent solution of the non-equilibrium Green function (NEGF) equations and Poisson equation. The NEGF equations are solved using the recursive Green function algorithm of [21], the quantum Jacobian of [22], and the boundary self-energies of [22]. A cross sectional view of the device used in our simulation is shown in Fig. 1.

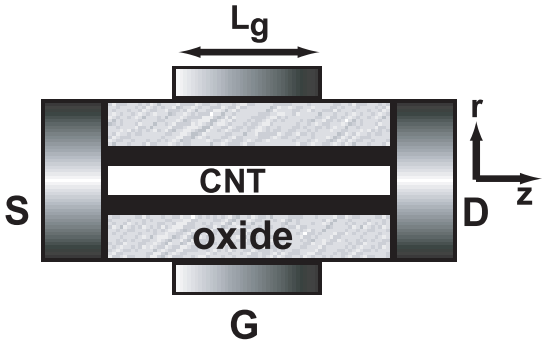

Figure 1: Device cross sectional view.

For this wrap-around structure, the potential V is independent of ϕ and Poisson equation in cylindrical coordinates

(r,ϕ,z) becomes

$$\frac{\partial^2 V}{\partial r^2} + \left(\frac{1}{r} + \frac{1}{\epsilon}\frac{\partial \epsilon}{\partial r}\right)\frac{\partial V}{\partial r} + \frac{\partial^2 V}{\partial z^2} = -\rho/\epsilon. \quad (1)$$

Spatial variation of permittivity is allowed in the radial direction only, and Eq. (1) is solved by standard Newton-Rapshon method with appropriate boundary conditions. The charge density in each atomic layer is calculated from the following equation

$$\rho_L = (2q)\int \frac{dE}{2\pi} Tr\left(f_S A^L_{L,L} + f_D\left[A_{L,L} - A^L_{L,L}\right]\right). \quad (2)$$

Here L is the atomic layer index, Tr is trace over the atomic orbitals, f_S and f_D are the source and drain Fermi functions and A's are the spectral functions calculated from the following equations

$$A^L_{L,L} = G_{L,1}\Gamma_{1,1}G^\dagger_{L,1} \quad (3)$$
$$A_{L,L} = i\left(G_{L,L} - G^\dagger_{L,L}\right),$$

where Γ is the broadening function and $G_{L,L}$ is the diagonal block of the Green function calculated from the recursive Green function algorithm [21]

$$G_{L,L} = g_{L,L} + g_{L,L}t_{L,L-1}G_{L-1,L-1}t_{L-1,L}g_{L,L}. \quad (4)$$

Here $g_{L,L}$ is the bare, right-connected Green function

$$g_{L,L} = \left(E - D_L - t_{L,L+1}g_{L+1,L+1}t_{L+1,L}\right)^{-1}, \quad (5)$$

where D_L is given by

$$D_L = H_L - U_L. \quad (6)$$

Here U_L is the appropriately shifted potential energy at the L^{th} atomic layer, H_L is the layer Hamiltonian, and t's are the layer to layer coupling matrices. The Hamiltonian matrix and the coupling matrices are formed using π-bond of carbon atoms under tight binding approximation. Once the self-consistency between the potential and the charge density is achieved, the current is calculated from

$$I = \frac{2q}{h}\int dE\, T\left(f_S - f_D\right), \quad (7)$$

where transmission is

$$T = Tr\left(\Gamma_{1,1}\left[A_{1,1} - G_{1,1}\Gamma_{1,1}G^\dagger_{1,1}\right]\right). \quad (8)$$

3 RESULTS AND DISCUSSIONS

For simulation we use a (13,0) zigzag CNT with diameter $\sim$ 1 nm and band gap of 0.76 eV. Fig. 2(a) shows the leakage current as a function of CNT length for 3 different geometries.

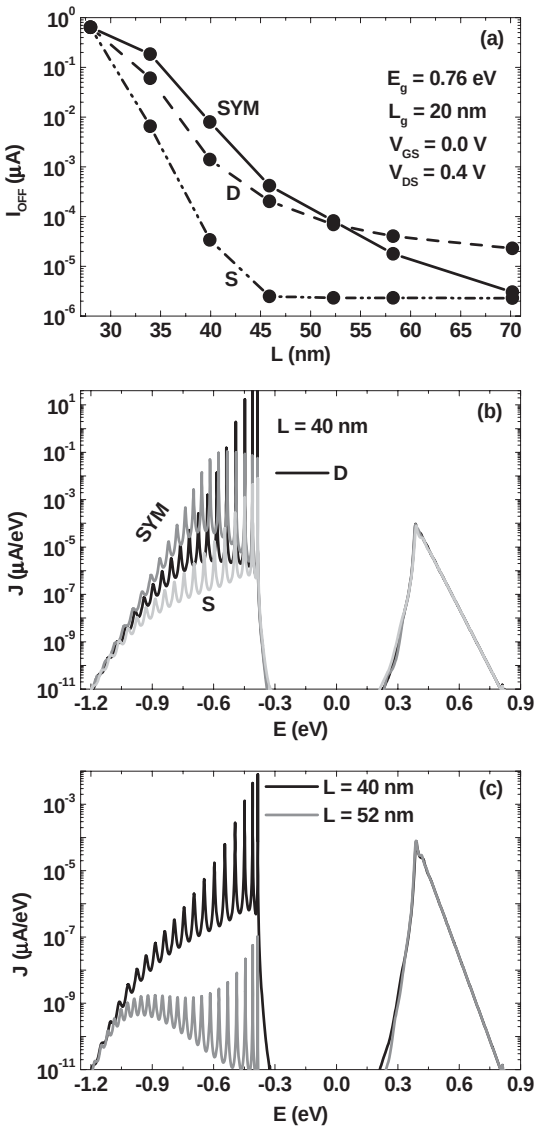

Figure 2: (a) I_{OFF} vs CNT length. (b) Current density vs energy for 3 devices with CNT length of 40 nm. (c) Current density plots in the S structure for 2 different values of CNT length.

The symmetric geometry (SYM) has the highest leakage current for $L < 50$ nm. Fixing the drain extension to 4 nm (D) results in the next highest leakage. Fixing the source extension to 4 nm (S) results in the lowest leakage. This configuration suppresses the interband tunneling component of the leakage current due to reduced electric field near the drain region. The physics is revealed in the plot of current density versus energy shown in Fig. 2(b). All three structures have the same intraband component but the interband component of the leakage current is least for the S structure. Also the

leakage current in structure S falls quickly with CNT length and saturates at a critical value of L. Fig 2(c) reveals the physics. Increasing L reduces the interband component of the leakage current but does not affect the intraband component of the leakage current. At large enough L, the intraband component dominates and further reduction of the interband component of the leakage current has no effect on the total.

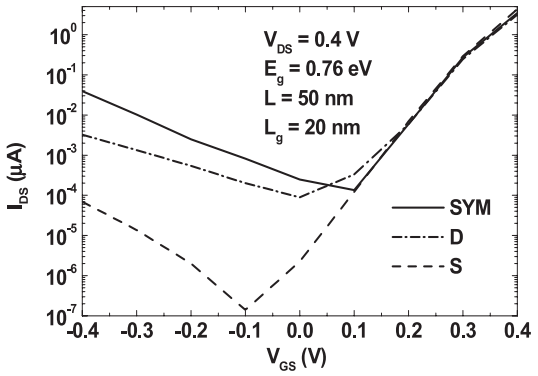

Figure 3: I_{DS} vs V_{GS} plots.

The I_{DS} vs V_{GS} plots for 3 different geometries with 50 nm CNT are shown in Fig. 3. The interband tunneling current at negative voltages is minimum with the gate close to the source (S). The turn-on current at positive voltages is unaffected by the symmetry. Therefore, the ON/OFF current ratio is maximum with the S structure. The components of the OFF current and the ON/OFF current ratio for different geometry with 50 nm CNT length are shown in Table 1.

Dev.	I_{OFF} (μA)	Interband	Intraband	ON/OFF
SYM	2.5×10^{-4}	2.4×10^{-4}	3.0×10^{-6}	1.4×10^{4}
D	9.0×10^{-5}	8.7×10^{-5}	2.9×10^{-6}	3.5×10^{4}
S	2.3×10^{-6}	3.6×10^{-9}	2.3×10^{-6}	1.9×10^{6}

Table 1: Statistics of the OFF current components and the ON/OFF current ratio for 3 devices.

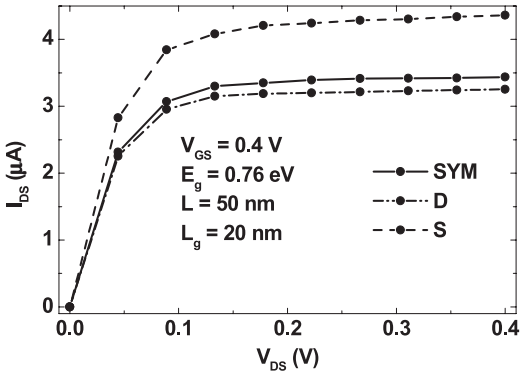

Figure 4: I-V characteristics.

Fig. 4 shows the I-V characteristics for 3 different structures. Regarding Fig. 3 and Fig. 4 we calculate the figures of merit, switching time $\tau_{\rm s}$, cutoff frequency $f_{\rm T}$, and small-signal gain $A_{\rm v}$ for 3 different geometries. The gate capacitance is calculated from $C_g = 2\pi R \int_0^{L_g} dz \frac{\delta D_r}{\delta V_g}$ where R is the radius of the dielectric, and the integral is over L_g. This expression includes the effect of the quantum capacitance also. Details about the calculation for 30 nm long CNT with 0.98 eV band gap has been discussed in our previous work [23]. The figures of merit are listed in Table 2.

Dev.	C_g (aF)	$\tau_{\rm s}$ (ps)	$f_{\rm T}$ (THz)	r_o (MΩ)	$A_{\rm v}$
SYM	0.2	23.5	25	2.95	93
D	0.42	53	11	4.1	118
S	0.41	39	15	2.2	88

Table 2: Figures of merit for 3 devices.

The increased capacitance resulting from the closer proximity of the gate to the source/drain increases the switching time and reduces the cutoff frequency. The electric field in the drain varies with geometry and changes the percent modulation of the intraband tunnel barrier length. The modulation is maximal for the structure with the gate close to the source. In this case the width of the triangular barrier to intraband tunneling is modulated by the voltage at the drain. For the D structure, the intraband tunnel barrier width is essentially a square barrier the length of the CNT. This increases r_o in the D structure but decreases in the S structure and hence change in $A_{\rm v}$. Even though the I-V characteristics of these ohmicly contacted CNTFETs look like those of a FET, the devices operate as voltage modulated tunnel barriers in which the bulk CNT itself, not the contacts, act as the tunnel barrier.

Considering the small gate capacitance and the resonant tunneling characteristic of the interband leakage current, we should also consider the effect of Coulomb blockade on the interband tunneling. The single electron charging energy is $U_e = e^2/2C$. Considering C_g as C the single electron charging energy with 0.41 aF (S structure) is 0.2 eV. This energy is much greater than the broadening energy (in the range of meV [24]) of the quantized states (Fig. 2). Therefore, Coulomb blockade effects should, in principle, move the turn-on of the I_{DS} vs V_{GS} curve of Fig. 3 due to interband tunneling, back to the left by 0.2 V and make the FETs effectively unipolar devices.

4 CONCLUSIONS

Geometry dependency of the leakage current for ohmicly contacted CNTFETs is analyzed. The geometry with the gate closer to the source provides the most blocking of the interband component of the leakage current, and it gives the highest ON/OF current ratio with inverse subthreshold ($\sim$

63 mV/dec) close to the ideal value of 60 mV/dec. The capacitance with asymmetric structure increases due to higher electric field near the contact.

5 ACKNOWLEDGEMENT

This work is supported by the NSF (DMR-0103248), DOD/DARPA/DMEA (DMEA90-02-2-0216), and the Microelectronics Advanced Research Corporation Focus Center on Nano Materials (FENA).

References

[1] J. Guo, S. Datta, M. Lundstrom, M. Brink, P. McEuen, A. Javey, H. Dai, H. Kim, and P. McIntyre, IEDM, IEEE, 2, 711–714, 2002.

[2] A. Javey, J. Guo, Q. Wang, M. Lundstrom, and H. Dai, Nature, 424, 654–657, 2003.

[3] A. Javey, J. Guo, M. Paulsson, Q. Wang, D. Mann, M. Lundstrom, and H. Dai, Phys. Rev. Lett., 92, 106804, 2004.

[4] A. Javey, J. Guo, D. B. Farmer, Q. Wang, D. Wang, R. G. Gordon, M. Lundstrom, and H. Dai, Nano Lett., 4, 447–450, 2004.

[5] A. Javey, J. Guo, D. B. Farmer, Q. Wang, E. Yenilmez, R. G. Gordon, M. Lundstrom, and H. Dai, Nano Lett., 4, 1319–1322, 2004.

[6] M. Radosavljevic, J. Appenzeller, and P. Avouris, Appl. Phys. Lett., 84, 3693–3695, 2004.

[7] X. Cui, M. Freitag, R. Martel, L. Brus, and P. Avouris, Nano Lett., 3, 783–787, 2003.

[8] S. Auvray, J. Borghetti, M. F. Goffman, A. Filoramo, V. Derycke, J. P. Bourgoin, and O. Jost, Appl. Phys. Lett., 84, 5106–5108, 2004.

[9] R. Martel, V. Derycke, C. Lavoie, J. Appenzeller, K. K. Chan, J. Tersoff, and P. Avouris, Phys. Rev. Lett., 87, 256805, 2001.

[10] A. Javey, M. Shim, and H. Dai, Appl. Phys. Lett., 80, 1064–1066, 2002.

[11] J. P. Clifford, D. L. John, and D. L. Pulfrey, IEEE Trans. NanoTech., 2, 181–185, 2003.

[12] J. Guo, S. Datta, and M. Lundstrom, IEEE Trans. Elec. Dev., 51, 172–177, 2004.

[13] J. Guo, J. Wang, E. Polizzi, S. Datta, and M. Lundstrom, IEEE Trans. Nanotech., 2, 329–334, 2003.

[14] S. Heinze, J. Tersoff, R. Martel, V. Derycke, J. Appenzeller, and P. Avouris, Phys. Rev. Lett., 89, 106801, 2002.

[15] R. M. Stoltenberg and A. T. Woolley, Biomedical Microdevices, 6, 105–111, 2004.

[16] K. Keren, R. S. Berman, E. Buchstab, U. Sivan, and E. Braun, Science, 302, 1380–1382, 2003.

[17] S. Heinze, M. Radosavljevic, J. Tersoff, and P. Avouris, Phys. Rev. B, 68, 235418(1–5), 2003.

[18] M. Radosavljevic, S. Heinze, J. Tersoff, and P. Avouris, Appl. Phys. Lett., 83, 2435–2437, 2003.

[19] S. Heinze, J. Tersoff, and P. Avouris, Appl. Phys. Lett., 83, 5038, 2003.

[20] Y. M. Lin, J. Appenzeller, and P. Avouris, Nano Lett., 4, 947, 2004.

[21] R. Lake, G. Klimeck, R. C. Bowen, and D. Jovanovic, J. Appl. Phys., 81, 7845–7869, 1997.

[22] R. Lake, G. Klimeck, R. C. Bowen, D. Jovanovic, D. Blanks, and M. Swaminathan, Phys. Stat. Sol. (b), 204, 354–357, 1997.

[23] K. Alam and R. Lake, (submitted).

[24] K. Alam and R. Lake, unpublished.